Phenomenological analysis of the double-pion production in nucleon-nucleon collisions up to 2.2 GeV

Xu Cao,[1,3,5,*] Bing-Song Zou,[2,3,4] and Hu-Shan Xu[1,3,4]

[1]*Institute of Modern Physics, Chinese Academy of Sciences, Lanzhou 730000, China*

[2]*Institute of High Energy Physics, Chinese Academy of Sciences, Beijing 100049, China*

[3]*Theoretical Physics Center for Sciences Facilities, Chinese Academy of Sciences, Beijing 100049, China*

[4]*Center of Theoretical Nuclear Physics, National Laboratory of Heavy Ion Collisions, Lanzhou 730000, China*

[5]*Graduate University of Chinese Academy of Sciences, Beijing 100049, China*

(Received 4 April 2010; published 3 June 2010)

With an effective Lagrangian approach, we analyze several $NN \to NN\pi\pi$ channels by including various resonances with mass up to 1.72 GeV. For the channels with the pion pair of isospin zero, we confirm the dominance of $N^*(1440) \to N\sigma$ in the near-threshold region. At higher energies and for channels with the final pion pair of isospin one, we find large contributions from $N^*(1440) \to \Delta\pi$, double-Δ, $\Delta(1600) \to N^*(1440)\pi$, $\Delta(1600) \to \Delta\pi$, and $\Delta(1620) \to \Delta\pi$. There are also sizable contributions from $\Delta \to \Delta\pi$, $\Delta \to N\pi$, $N \to \Delta\pi$, and nucleon pole at energies close to the threshold. We give a good reproduction to the total cross sections up to beam energies of 2.2 GeV except for the $pp \to pp\pi^0\pi^0$ channel at energies around 1.1 GeV and our results agree with the existing data of differential cross sections of $pp \to pp\pi^+\pi^-$, $pp \to nn\pi^+\pi^+$, and $pp \to pp\pi^0\pi^0$ which are measured at CELSIUS and COSY.

DOI: 10.1103/PhysRevC.81.065201 PACS number(s): 13.75.Cs, 14.20.Gk, 25.75.Dw

I. INTRODUCTION

Double-pion production in both pion- and photo-induced reactions has been an intriguing field to study baryon spectrum and has given insight to the properties of strong interaction [1,2]. These reactions close to threshold are also an interesting area to test chiral symmetry and have been extensively explored experimentally [3] and theoretically [4]. Recently the double-pion production in the electro-production off protons has advanced an important step [5]. All essential contributions are identified from the data and the major isobar channels are well determined. On the other hand, as another fascinating platform for studying resonances properties, double-pion production in nucleon-nucleon collisions has been accurately measured at the facilities of CELSIUS and COSY in the past few years, and the comprehensive data of various differential cross sections are obtained up to beam energies 1.3 GeV [6–11]. However, on the theoretical side, the study of this reaction is scarce. The state-of-art one is still the Valencia model calculation [12] of more than 10 years ago after some much earlier calculations of one-pion exchange (OPE) model [13] of more than 45 years ago. Thus, a more comprehensive analysis matching the modern data is very necessary.

The early OPE model, which mainly focused on the old data at beam energies of 2.0 and 2.85 GeV [14], included two types of diagrams with the final two pions produced from a single and two baryon line(s), respectively. It used the amplitudes of $\pi N \to \pi\pi N$ and $\pi N \to \pi N$ extracted from limited data and the off-shell corrections were considered under several assumptions. It did not account for the explicit production mechanisms of double-pion and other exchanged meson besides π-meson. The Valencia model is characteristic by the dominance of $N^*(1440) \to N\sigma$ in the near-threshold region in the isospin-allowed channels while the double-Δ and $N^*(1440) \to \Delta\pi$ rise up at higher energies and in channels where $N^*(1440) \to N\sigma$ is forbidden by the isospin conservation. Recently, the experimental data [6,9] confirm the predicted behavior close to threshold and this makes $pp \to pp\pi^+\pi^-$ and $pp \to pp\pi^0\pi^0$ good places to study $N^*(1440)$ whose structure is still controversial. Current data seem to show a weaker $N^*(1440) \to \Delta\pi$ than that listed in Particle Data Group [15] and support the explanation of $N^*(1440)$ as the monopole excitation of the nucleon. Contrarily, the case is much more complicated at higher energies. The dominance of the double-Δ mechanism in the Valencia model results in that the total cross section of $pp \to pp\pi^0\pi^0$ is about a factor of four larger than that of $pp \to nn\pi^+\pi^+$, while the new exclusive and the old bubble-chamber data are consistent to conclude an approximate equal value of these two channels. The isospin decomposition unambiguously reveal that more isospin $3/2$ resonances besides Δ is required to explain the data [6,8], and this is also the reason that the Valencia model including simply the $N^*(1440)$ and Δ achieved merely a rough agreement in most channels. Indeed, at higher energies the contribution from higher lying resonances, especially those having large double-pion decay channels, should become relevant. The recent detailed measurements performed by CELSIUS and COSY make the further exploration of these problems possible.

In the present work, we try to incorporate the resonances with mass up to 1.72 GeV in an effective Lagrangian model with the motivation to give a reasonable explanation to the six isospin channels of $NN \to NN\pi\pi$ simultaneously and get better understanding of dynamics for this kind of reaction. Our paper is organized as follows. In Sec. II, we present the formalism and ingredients in our computation. The numerical results and discussion are demonstrated in Sec. III and a brief summary is given in Sec. IV.

*caoxu@impcas.ac.cn

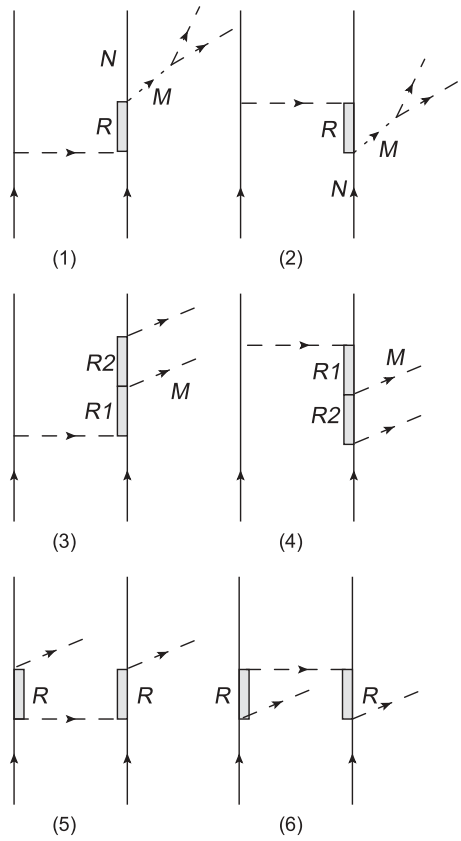

FIG. 1. Feynman diagrams for $NN \to NN\pi\pi$. The solid, dashed, and dotted lines stand for the nucleon, mesons, and intermediate σ (or ρ)-meson. The shading histograms represent the intermediate resonances or nucleon poles. In the text, we use $R \to NM$, $R1 \to R2M$ and double-R to label (1)(2), (3)(4), and (5)(6), respectively.

II. FORMALISM AND INGREDIENTS

We consider the Feynman diagrams as depicted in Fig. 1, and exchanged diagrams are also included. The diagrams in which one of the pions is pre-emitted followed by the excitation and de-excitation of resonances were shown to be very small in the Valencia model [12], hence we neglect them here. We find that the pre-emission diagrams of Figs. 1(2), 1(4), and 1(6) are also negligibly small, consistent with the Valencia model, so we do not include them either in our later concrete computation.

We use the commonly used interaction Lagrangians for πNN, $\pi\Delta\Delta$, ηNN, σNN, and ρNN couplings,

$$\mathcal{L}_{\pi NN} = -\frac{f_{\pi NN}}{m_\pi}\overline{N}\gamma_5\gamma_\mu\vec{\tau}\cdot\partial^\mu\vec{\pi}N, \tag{1}$$

$$\mathcal{L}_{\pi\Delta\Delta} = \frac{f_{\pi\Delta\Delta}}{m_\pi}\overline{\Delta}^\nu\gamma_5\gamma_\mu\vec{\tau}\cdot\partial^\mu\vec{\pi}\Delta_\nu + \text{h.c.}, \tag{2}$$

$$\mathcal{L}_{\eta NN} = -ig_{\eta NN}\overline{N}\gamma_5\eta N, \tag{3}$$

$$\mathcal{L}_{\sigma NN} = g_{\sigma NN}\overline{N}\sigma N, \tag{4}$$

$$\mathcal{L}_{\rho NN} = -g_{\rho NN}\overline{N}\left(\gamma_\mu + \frac{\kappa}{2m_N}\sigma_{\mu\nu}\partial^\nu\right)\vec{\tau}\cdot\vec{\rho}^\mu N. \tag{5}$$

At each vertex a relevant off-shell form factor is used. In our calculation, we take the same form factors as that used in the Bonn potential model [16],

$$F_M^{NN}(k_M^2) = \left(\frac{\Lambda_M^2 - m_M^2}{\Lambda_M^2 - k_M^2}\right)^n, \tag{6}$$

with $n = 1$ for π- and η-meson and $n = 2$ for ρ-meson. k_M, m_M, and Λ_M are the four-momentum, mass, and cutoff parameters for the exchanged meson, respectively. The coupling constants and the cutoff parameters are taken as [16–18]: $f_{\pi NN}^2/4\pi = 0.078$, $g_{\eta NN}^2/4\pi = 0.4$, $g_{\sigma NN}^2/4\pi = 5.69$, $g_{\rho NN}^2/4\pi = 0.9$, $\Lambda_\pi = \Lambda_\eta = 1.0$ GeV, $\Lambda_\sigma = 1.3$ GeV, $\Lambda_\rho = 1.6$ GeV, and $\kappa = 6.1$. We use $f_{\pi\Delta\Delta} = 4f_{\pi NN}/5$ from the quark model [1,12]. The mass and width of σ-meson are adopted as 550 and 500 MeV, respectively.

We include all N^* and Δ^* resonances with spin-parity $1/2^\pm$, $3/2^\pm$, $5/2^\pm$, and mass up to 1.72 GeV listed in Particle Data Group (PDG) tables [15]. The resonances with further higher masses are expected to give negligible contributions in the energy region considered here and their two pion branching ratios have large uncertainties, so we do not include them at present. The effective Lagrangians for the relevant resonance couplings are [19,20],

$$\mathcal{L}_{\pi NR}^{1/2^+} = g_{\pi NR}\overline{N}\gamma_5\gamma_\mu\vec{\tau}\cdot\partial^\mu\vec{\pi}R + \text{h.c.}, \tag{7}$$

$$\mathcal{L}_{\eta NR}^{1/2^+} = g_{\eta NR}\overline{N}\gamma_5\eta R + \text{h.c.}, \tag{8}$$

$$\mathcal{L}_{\sigma NR}^{1/2^+} = g_{\sigma NR}\overline{N}\sigma R + \text{h.c.}, \tag{9}$$

$$\mathcal{L}_{\rho NR}^{1/2^+} = g_{\rho NR}\overline{N}\gamma_\mu\vec{\tau}\cdot\vec{\rho}^\mu R + \text{h.c.}, \tag{10}$$

$$\mathcal{L}_{\pi\Delta R}^{1/2^+} = g_{\pi\Delta R}\overline{\Delta}_\mu\vec{\tau}\cdot\partial^\mu\vec{\pi}R + \text{h.c.}, \tag{11}$$

$$\mathcal{L}_{\pi NR}^{1/2^-} = g_{\pi NR}\overline{N}\vec{\tau}\cdot\vec{\pi}R + \text{h.c.}, \tag{12}$$

$$\mathcal{L}_{\eta NR}^{1/2^-} = g_{\eta NR}\overline{N}\eta R + \text{h.c.}, \tag{13}$$

$$\mathcal{L}_{\rho NR}^{1/2^-} = g_{\rho NR}\overline{N}\gamma_5\left(\gamma_\mu - \frac{q_\mu \not{q}}{q^2}\right)\vec{\tau}\cdot\vec{\rho}^\mu R + \text{h.c.}, \tag{14}$$

$$\mathcal{L}_{\pi\Delta R}^{1/2^-} = g_{\pi\Delta R}\overline{\Delta}_\mu\gamma_5\vec{\tau}\cdot\partial^\mu\vec{\pi}R + \text{h.c.}, \tag{15}$$

$$\mathcal{L}_{\pi NR}^{3/2^+} = g_{\pi NR}\overline{N}\vec{\tau}\cdot\partial^\mu\vec{\pi}R_\mu + \text{h.c.}, \tag{16}$$

$$\mathcal{L}_{\eta NR}^{3/2^+} = g_{\eta NR}\overline{N}\partial^\mu\eta R_\mu + \text{h.c.}, \tag{17}$$

$$\mathcal{L}_{\rho NR}^{3/2^+} = g_{\rho NR}\overline{N}\gamma_5\vec{\tau}\cdot\vec{\rho}^\mu R_\mu + \text{h.c.}, \tag{18}$$

$$\mathcal{L}_{\pi\Delta R}^{3/2^+} = g_{\pi\Delta R}\overline{\Delta}^\mu\gamma_5\vec{\tau}\cdot\vec{\pi}R_\mu + \text{h.c.}, \tag{19}$$

$$\mathcal{L}_{\pi N^*(1440)R}^{3/2^+} = g_{\pi N^*R}\overline{N^*}\vec{\tau}\cdot\partial^\mu\vec{\pi}R_\mu + \text{h.c.}, \tag{20}$$

$$\mathcal{L}_{\pi NR}^{3/2^-} = g_{\pi NR}\overline{N}\gamma_5\gamma_\mu\vec{\tau}\cdot\partial^\mu\partial^\nu\vec{\pi}R_\nu + \text{h.c.}, \tag{21}$$

$$\mathcal{L}_{\rho NR}^{3/2^-} = g_{\rho NR}\overline{N}\vec{\tau}\cdot\vec{\rho}^\mu R_\mu + \text{h.c.}, \tag{22}$$

$$\mathcal{L}_{\pi\Delta R}^{3/2^-} = g_{\pi\Delta R}\overline{\Delta}^\mu\gamma_\nu\vec{\tau}\cdot\partial^\nu\vec{\pi}R_\mu + \text{h.c.}, \tag{23}$$

$$\mathcal{L}_{\pi NR}^{5/2^+} = g_{\pi NR}\overline{N}\gamma_5\gamma_\mu\vec{\tau}\cdot\partial^\mu\partial^\nu\partial^\lambda\vec{\pi}R_{\nu\lambda} + \text{h.c.}, \tag{24}$$

$$\mathcal{L}_{\rho NR}^{5/2^+} = g_{\rho NR}\overline{N}\left(p_N^\mu - \frac{p_N\cdot p_R p_R^\mu}{p_R^2}\right)\vec{\tau}\cdot\vec{\rho}^\nu R_{\mu\nu} + \text{h.c.}, \tag{25}$$

$$\mathcal{L}_{\sigma NR}^{5/2^+} = g_{\sigma NR}\overline{N}\partial^\mu\partial^\nu\sigma R_{\mu\nu} + \text{h.c.}, \tag{26}$$

$$\mathcal{L}_{\pi\Delta R}^{5/2^+} = g_{\pi\Delta R}\overline{\Delta}_\mu\vec{\tau}\cdot\partial^\mu\partial^\nu\partial^\lambda\vec{\pi}R_{\nu\lambda} + \text{h.c.}, \tag{27}$$

$$\mathcal{L}^{5/2^-}_{\pi NR} = g_{\pi NR}\overline{N}\vec{\tau}\cdot\partial^\mu\partial^\nu\vec{\pi}R_{\mu\nu} + \text{h.c.}, \quad (28)$$

$$\mathcal{L}^{5/2^-}_{\pi\Delta R} = g_{\pi\Delta R}\overline{\Delta}_\mu\gamma_5\vec{\tau}\cdot\partial^\mu\partial^\nu\partial^\lambda\vec{\pi}R_{\nu\lambda} + \text{h.c.}, \quad (29)$$

For the resonance-nucleon-meson vertices, form factors with the following form are used:

$$F^{RN}_M(k^2_M) = \left(\frac{\Lambda^{*2}_M - m^2_M}{\Lambda^{*2}_M - k^2_M}\right)^n, \quad (30)$$

with $n = 1$ for N^* resonances and $n = 2$ for Δ resonances. We employ $\Lambda^*_\pi = \Lambda^*_\sigma = \Lambda^*_\eta = \Lambda^*_\rho = 1.0$ for all resonances except $\Lambda^*_\pi = 0.8$ for $\Delta^*(1600)$. We also use Blatt-Weisskopf barrier factors $B(Q_{N^*\Delta\pi})$ in the $N^*(1440)$-Δ-π vertices [21],

$$B(Q_{N^*\Delta\pi}) = \sqrt{\frac{P^2_{N^*\Delta\pi} + Q^2_0}{Q^2_{N^*\Delta\pi} + Q^2_0}}. \quad (31)$$

Here, Q_0 is the hadron scale parameter $Q_0 = 0.197327/R$ GeV/c, where R is the radius of the centrifugal barrier in the unit of fm and is tuned to be 1.5 fm to fit the data. $Q_{N^*\Delta\pi}$ and $P_{N^*\Delta\pi}$ is defined as,

$$Q^2_{N^*\Delta\pi} = \frac{(s^*_N + s_\Delta - s_\pi)^2}{4s^*_N} - s_\Delta, \quad (32)$$

$$P^2_{N^*\Delta\pi} = \frac{\left(m^2_{N^*} + m^2_\Delta - m^2_\pi\right)^2}{4m^2_{N^*}} - m^2_\Delta, \quad (33)$$

with s_x being the invariant energy squared of x particle. Because the mass of σ-meson is near the two-π threshold, the following Lagrangians and form factor are employed for the σ-π-π vertex [1,2,22],

$$\mathcal{L}_{\sigma\pi\pi} = g_{\sigma\pi\pi}\partial^\mu\vec{\pi}\cdot\partial_\mu\vec{\pi}\sigma, \quad (34)$$

$$\mathcal{L}_{\rho\pi\pi} = g_{\rho\pi\pi}\vec{\pi}\times\partial_\mu\vec{\pi}\cdot\vec{\rho}^\mu, \quad (35)$$

$$F^{\pi\pi}_\sigma(\vec{q}^2) = \left(\frac{\Lambda^2 + \Lambda^2_0}{\Lambda^2 + \vec{q}^2}\right)^2, \quad (36)$$

where $\vec{q}$ is the relative momentum of the emitted pion in the center of mass system. We use $\Lambda = 0.8$ GeV and $\Lambda^2_0 = 0.12$ GeV^2 to normalize this form factor to unity when π- and σ-meson are all on-shell. The decay width of $\sigma \to \pi\pi$ and $\rho \to \pi\pi$ yield $g^2_{\sigma\pi\pi} = 6.06$ and $g^2_{\rho\pi\pi} = 2.91$.

The form factor for the resonance, $F_R(q^2)$, is taken as,

$$F_R(q^2) = \frac{\Lambda^4_R}{\Lambda^4_R + \left(q^2 - M^2_R\right)^2}, \quad (37)$$

with $\Lambda_R = 1.0$ GeV. The same type of form factors are also applied to the nucleon pole with $\Lambda_N = 0.8$ GeV. The propagators of the exchanged meson, nucleon pole, and resonance can be written as [16,17],

$$G_{\pi/\eta}(k_{\pi/\eta}) = \frac{i}{k^2_{\pi/\eta} - m^2_{\pi/\eta}}, \quad (38)$$

$$G_\sigma(k_\sigma) = \frac{i}{k^2_\sigma - m^2_\sigma + im_\sigma\Gamma_\sigma}, \quad (39)$$

$$G^{\mu\nu}_\rho(k_\rho) = -i\frac{g^{\mu\nu} - k^\mu_\rho k^\nu_\rho/k^2_\rho}{k^2_\rho - m^2_\rho}, \quad (40)$$

$$G_N(q) = \frac{-i(\not{q} + m_N)}{q^2 - m^2_N}. \quad (41)$$

$$G^{1/2}_R(q) = \frac{-i(\not{q} + M_R)}{q^2 - M^2_R + iM_R\Gamma_R}. \quad (42)$$

$$G^{3/2}_R(q) = \frac{-i(\not{q} + M_R)G_{\mu\nu}(q)}{q^2 - M^2_R + iM_R\Gamma_R}. \quad (43)$$

$$G^{5/2}_R(q) = \frac{-i(\not{q} + M_R)G_{\mu\nu\alpha\beta}(q)}{q^2 - M^2_R + iM_R\Gamma_R}. \quad (44)$$

Here, Γ_R is the total width of the corresponding resonance, and $G_{\mu\nu}(q)$ and $G_{\mu\nu\alpha\beta}(q)$ are defined as,

$$G_{\mu\nu}(q) = -g_{\mu\nu} + \frac{1}{3}\gamma_\mu\gamma_\nu + \frac{1}{3M_R}(\gamma_\mu q_\nu - \gamma_\nu q_\mu) + \frac{2}{3M^2_R}q_\mu q_\nu, \quad (45)$$

$$G_{\mu\nu\alpha\beta}(q) = -\frac{1}{2}(\tilde{g}_{\mu\alpha}\tilde{g}_{\nu\beta} + \tilde{g}_{\mu\beta}\tilde{g}_{\nu\alpha}) + \frac{1}{5}\tilde{g}_{\mu\nu}\tilde{g}_{\alpha\beta} \quad (46)$$

$$-\frac{1}{10}(\tilde{\gamma}_\mu\tilde{\gamma}_\alpha\tilde{g}_{\nu\beta} + \tilde{\gamma}_\nu\tilde{\gamma}_\beta\tilde{g}_{\mu\alpha} + \tilde{\gamma}_\mu\tilde{\gamma}_\beta\tilde{g}_{\nu\alpha} + \tilde{\gamma}_\nu\tilde{\gamma}_\alpha\tilde{g}_{\mu\beta}), \quad (47)$$

$$\tilde{g}_{\mu\nu}(q) = -g_{\mu\nu} + \frac{q_\mu q_\nu}{M^2_R}, \quad \tilde{\gamma}_\mu = -\gamma_\mu + \frac{\not{q}q_\mu}{M^2_R}. \quad (48)$$

Because constant width is used in the Breit-Wigner (BW) formula, we adopt the pole positions of various resonances for parameters appearing in the propagators.

The coupling constants appearing in relevant resonances are determined by the empirical partial decay width of the resonances taken from PDG [15], and then we adjust the values of cutoff in form factors to fit the data. The relations between the branching ratios of the adopted resonances and the corresponding coupling constants squared can be calculated straightforwardly with above Lagrangians, and most of them can be found in the appendix of Ref. [17]. The detailed calculations of $g_{\rho NR}$ and $g_{\sigma NR}$ from the $R \to N\rho(\sigma) \to N\pi\pi$ decay are given in Ref. [23]. The values of coupling constants used in our computation are compiled in the Table I, together with the properties of the resonances and the central value of branch ratios. It should be noted that we adopt nearly half of the decay width of $N^*(1440) \to \Delta\pi$ in PDG as the recent data favored [6,9,24].

Then the amplitudes can be obtained straightforwardly by applying the Feynman rules to Fig. 1. As to the different isospin channels, isospin coefficients are considered. We do not include the interference terms among different diagrams because their relative phases are not known, and the Valencia model seems to show that such terms are very small. The multiparticle phase space integration weighted by the amplitude squared can be performed by a Monte Carlo program using the code FOWL from the CERN program library [25].

III. NUMERICAL RESULTS AND DISCUSSION

As a starting point, in Fig. 2 we demonstrate our calculated total cross sections of six isospin channels compared with the existing data [6,9–11,14]. Our numerical results

TABLE I. Relevant parameters used in our calculation. The masses, widths, and branching ratios (BR) are taken from central values of PDG [15] except the BR for $N^*(1440) \to \Delta\pi$.

Resonance	Pole position	BW Width	Decay mode	Decay ratio	$g^2/4\pi$
$\Delta^*(1232)P_{33}$	(1210, 100)	118	$N\pi$	1.0	19.54
$N^*(1440)P_{11}$	(1365, 190)	300	$N\pi$	0.65	0.51
			$N\sigma$	0.075	3.20
			$\Delta\pi$	0.135	4.30
$N^*(1520)D_{13}$	(1510, 110)	115	$N\pi$	0.6	1.73
			$N\rho$	0.09	1.32
			$\Delta\pi$	0.2	0.01
$N^*(1535)S_{11}$	(1510, 170)	150	$N\pi$	0.45	0.037
			$N\eta$	0.525	0.34
			$N\rho$	0.02	0.15
$\Delta^*(1600)P_{33}$	(1600, 300)	350	$N\pi$	0.175	1.09
			$\Delta\pi$	0.55	59.9
			$N^*(1440)\pi$	0.225	289.1
$\Delta^*(1620)S_{31}$	(1600, 118)	145	$N\pi$	0.25	0.06
			$N\rho$	0.14	0.37
			$\Delta\pi$	0.45	83.7
$N^*(1650)S_{11}$	(1655, 165)	165	$N\pi$	0.775	0.06
			$N\eta$	0.065	0.026
			$N\rho$	0.08	0.011
			$\Delta\pi$	0.04	0.063
$N^*(1675)D_{15}$	(1660, 135)	150	$N\pi$	0.4	2.16
			$\Delta\pi$	0.55	3077.5
$N^*(1680)F_{15}$	(1675, 120)	130	$N\pi$	0.675	5.53
			$N\sigma$	0.125	4.45
			$N\rho$	0.09	0.32
			$\Delta\pi$	0.1	9.39
$N^*(1700)D_{13}$	(1680, 100)	100	$N\pi$	0.1	0.075
			$N\rho$	0.07	0.043
			$\Delta\pi$	0.04	0.003
$\Delta^*(1700)D_{33}$	(1650, 200)	300	$N\pi$	0.15	1.02
			$N\rho$	0.125	0.69
			$\Delta\pi$	0.45	0.072
$N^*(1710)P_{11}$	(1720, 230)	100	$N\pi$	0.15	0.012
			$N\eta$	0.062	0.042
			$N\sigma$	0.25	0.085
			$N\rho$	0.15	36.1
			$\Delta\pi$	0.275	0.12
$N^*(1720)P_{13}$	(1675, 195)	200	$N\pi$	0.15	0.12
			$N\eta$	0.04	0.28
			$N\rho$	0.775	190.7

give an overall good reproduction to all six channels. In Fig. 2 we do not show the following negligible contributions: double-N^*, $N^* \to N\rho$, $N^* \to N\pi$, $N^*(1520) \to \Delta\pi$, $N^*(1650) \to \Delta\pi$, $N^*(1675) \to \Delta\pi$, $N^*(1680) \to \Delta\pi$, $N^*(1680) \to N\sigma$, $N^*(1700) \to \Delta\pi$, $N^*(1710) \to \Delta\pi$, $N^*(1710) \to N\sigma$, double-$\Delta^*(1600)$, $\Delta^*(1600) \to N\pi$, double-$\Delta^*(1620)$, $\Delta^*(1620) \to N\rho$, $\Delta^*(1620) \to N\pi$, double-$\Delta^*(1700)$, $\Delta^*(1700) \to N\rho$, $\Delta^*(1700) \to N\pi$, and $\Delta^*(1700) \to \Delta\pi$. These terms are minor either because of their small branching ratios of double-pion channel such as $N^*(1535)$, $N^*(1650)$, and $N^*(1700)$, or belonging to higher partial waves such as $N^*(1520)$ and $N^*(1675)$, or lying beyond the considered energies such as $N^*(1680)$, $\Delta^*(1700)$, $N^*(1710)$, and $N^*(1720)$. It should be mentioned that ρ-meson exchange is much smaller than π-meson exchange in the available diagrams except for nucleon poles but we still include the ρ-meson exchange in the calculation for the completeness of our model.

Our results underestimate the data in the close-to-threshold region where the final-state interactions (FSI) should be relevant. We do not consider the initial-state interaction (ISI) either, because at present we do not have an unambiguous method at hand to simultaneously include the FSI and ISI in our model. The ISI usually has a weak energy dependence, so adjusting cutoff parameters in the form factors may partly account for it effectively [20]. We will give some qualitative observations of FSI in Sec. III E while in other sections the FSI as well as the ISI are not included in the presented results.

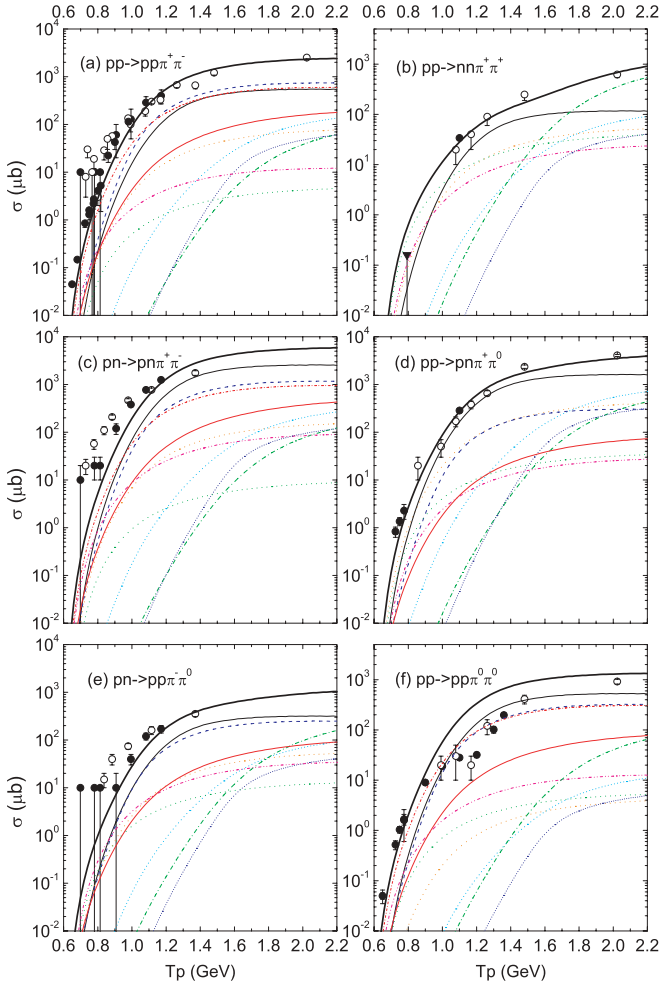

FIG. 2. (Color online) Total cross sections of $NN \to NN\pi\pi$. The black solid, red short-dash-dotted, blue dashed, orange dotted, green dotted, cyan short-dashed, green dash-dotted, royal short-dotted, magenta dash-dot-dotted, bold red, and bold solid curves correspond to contribution from double-Δ, $N^*(1440) \to N\sigma$, $N^*(1440) \to \Delta\pi$, $\Delta \to \Delta\pi$, $\Delta \to N\pi$, $\Delta^*(1600) \to \Delta\pi$, $\Delta^*(1600) \to N^*(1440)\pi$, $\Delta^*(1620) \to \Delta\pi$, nucleon pole, $N \to \Delta\pi$, and the full contributions, respectively. The solid circles and triangles represent the data from Ref. [6,9–11]. The open circles represent the old data [14].

Next we shall first address the $pp \to nn\pi^+\pi^+$ channel because it has negligible N^* contribution to be more clean. Then we shall discuss other channels and explore the different situation at each channel. In the following we assume the same definitions of various differential cross sections as graphically illustrated in the experimental articles [6,8]. The M_{ij} and M_{ijk} are the invariant mass spectra, and the angular distributions are all defined in the overall center-of-mass system. The Θ_M is the scattering angle of M, and δ_{ij} is the opening angle between i and j particles. The Θ_i^{ij} (or ϑ_i^{ij} corresponding to $\widehat{\Theta}_i^{ij}$ defined in Ref. [6,8]) is the scattering angle of i in the rest frame of i and j with respect to the beam axis (or the sum of momenta of i and j). The values of vertical axis are all arbitrarily normalized.

A. The channel of $pp \to nn\pi^+\pi^+$

The total cross section of this channel is demonstrated in Fig. 2(b). We find that the $\Delta \to N\pi \to N\pi\pi$ term is dominant below 1000 MeV while the $\Delta \to \Delta\pi$ and double-nucleon-pole terms are also important. The $\Delta \to N\pi \to N\pi\pi$ term is not included in the Valencia model [12]. Our model seems to overestimate the COSY-TOF upper limit by a factor of around four. The $\Delta \to \Delta\pi$ terms in two models are consistent with each other because we use the same coupling constant of $\pi\Delta\Delta$ from quark model but our double-Δ term contributes smaller as we use a smaller cutoff parameter in $\pi N\Delta$ form factor. Between 1000 and 1700 MeV, the contribution of the double-Δ term is the most important one, and the $n\pi^+$ invariant mass distribution at 1100 MeV does show a clear Δ peak as can be seen in Fig. 3. We also find that the $\Delta \to N\pi \to N\pi\pi$ and $\Delta \to \Delta\pi$ terms are crucial to get the right shape of differential cross sections at 1100 MeV in Fig. 3. Though the data is of poor statistics, the $\pi^+\pi^+$ invariant mass spectrum does not show obvious low-mass peak and this is realized by the inclusion of the $\Delta \to N\pi \to N\pi\pi$ and $\Delta \to \Delta\pi$ in our model. The $\cos\delta_{\pi\pi}$ distribution in Fig. 3(h) has also got a significant improvement compared to the results with the double-Δ term alone. These distributions should be very useful to constrain the poorly known coupling constant of $\pi\Delta\Delta$. The particular enhancement compared to our model without FSI in the nn invariant mass spectrum is probably an indication of strong ^1S_0nn FSI.

As can be seen in Fig. 2(b), the contribution from $\Delta^*(1600) \to N^*(1440)\pi$ term has a steep rise and begins to take over as the largest one for T_p above 1700 MeV. Besides, at large energies contributions from the $\Delta^*(1600) \to \Delta\pi$ and $\Delta^*(1620) \to \Delta\pi$ become significant. So in this energy region of $pp \to nn\pi^+\pi^+$, it is a good place to explore the properties of these Δ^* resonances. We would like to point out that these behaviors together with the dominance of $\Delta \to$

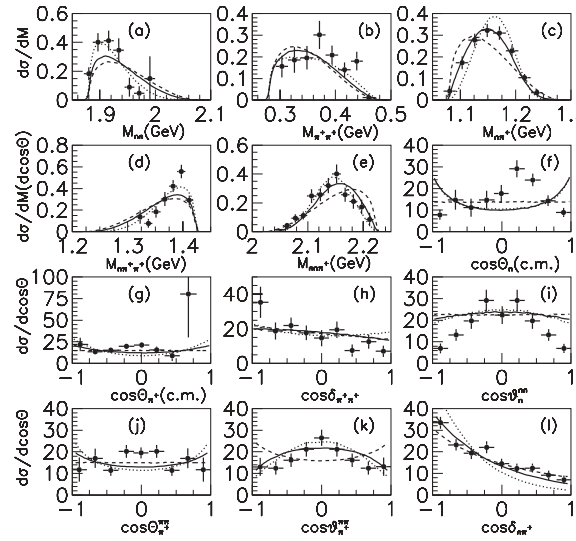

FIG. 3. Differential cross sections of $pp \to nn\pi^+\pi^+$ at beam energies 1100 MeV. The dashed, dotted, and solid curves correspond to the phase space, double- Δ, and full model distributions, respectively. The data are from Ref. [8].

$N\pi \to N\pi\pi$ and $\Delta \to \Delta\pi$ close to threshold alleviate the isospin problem of the $pp \to nn\pi^+\pi^+$ and $pp \to pp\pi^0\pi^0$ channels mentioned at the beginning of our article, because the isospin coefficients of these terms in $pp \to nn\pi^+\pi^+$ are bigger than that in $pp \to pp\pi^0\pi^0$ channel and this is contrary to the case of double-Δ. As a result, we get an improvement on the description of all isospin channels.

It should be addressed that it is very useful to pin down the cutoff values in form factors of the relevant Δ and Δ^* contributions using the data of $pp \to nn\pi^+\pi^+$ at first, and then it makes it much easier for us to determine the N^* contributions in other channels. The new value of total cross section of $pp \to nn\pi^+\pi^+$ measured at CELSIUS [6] is in line with previous data and this gives us some confidence on the extracted parameters. Further accurate measurements of the $pp \to nn\pi^+\pi^+$ channel should be very helpful for the improvement of the model.

B. The channel of $pp \to pp\pi^+\pi^-$

In Fig. 2(a) we can see that below 1000 MeV the $N^*(1440) \to N\sigma$ term is the largest while the $N^*(1440) \to \Delta\pi$ term is the second. In Figs. 4(a) and 4(b) it is demonstrated that the contribution of σ-meson exchange is larger than that of π-meson exchange in both the $N^*(1440) \to N\sigma$ and $N^*(1440) \to \Delta\pi$ diagrams and this shows the importance of isoscalar excitation of $N^*(1440)$. As depicted in Fig. 2(a), the double-Δ term is negligible at low energies as well as the $\Delta \to \Delta\pi$ term. Contributions from the nucleon pole and $N \to \Delta\pi$ terms are visible below 700 MeV. The proton and pion angular distributions in the center-of-mass system at 650 and 680 MeV are trivially isotropic and the model does agree with the measured data [6]. So we do not show them here. The differential cross sections at 750, 775, 800, and 895 MeV are given in Figs. 5, 6, 7, and 8, respectively. Our model calculations reproduce the published data well and are also compatible to the very preliminary data of CELSIUS at 895 MeV [8] as shown in Fig. 8. The role of $N^*(1440) \to \Delta\pi$ is evident in invariant mass spectrums and the data are fitted better than those including $N^*(1440) \to N\sigma$ alone. Most obviously, in Figs. 5–7, the anisotropic shape of $\vartheta_{\pi^+}^{\pi\pi}$ is well fitted after including the $N^*(1440) \to \Delta\pi$ while $N^*(1440) \to N\sigma$ term is symmetric, so $\vartheta_{\pi^+}^{\pi\pi}$ together with $\vartheta_{\pi^+}^{p\pi^+}$ and $\vartheta_{\pi^-}^{p\pi^-}$ is used to determined the ratio of partial decay widths of $N^*(1440) \to \Delta\pi$ and $N^*(1440) \to N\sigma$ [6]. The extracted value of this ratio from data strongly depends on the assumed mass of $N^*(1440)$, but consistently turns out to be smaller than that given by the PDG. This is believed to support the breathing mode of $N^*(1440)$ [26]. The FSI is evident in pp invariant mass spectrum, but seems to be much weaker than in the case of the $pp \to nn\pi^+\pi^+$ channel.

In the Valencia model the double-Δ is dominant above 1300 MeV. However, because we use smaller cutoff parameter for the $\pi N\Delta$ form factor in order to fit both $nn\pi^+\pi^+$ and $pp\pi^0\pi^0$ channels, in Fig. 2(a) our model shows that $N^*(1440) \to \Delta\pi$ begins to take over above 1100 MeV, and double-Δ and $N^*(1440) \to N\sigma$ are also important and comparable. We give the differential cross sections at 1100 and

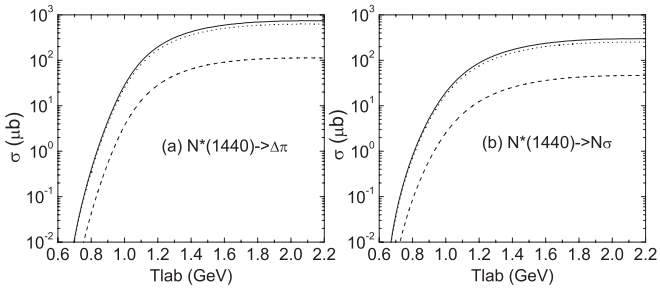

FIG. 4. The $N^*(1440) \to \Delta\pi$, $N^*(1440) \to N\sigma$ terms of $pp \to pp\pi^+\pi^-$. The dashed, dotted, and solid curves correspond to π-meson exchange, σ-meson exchange, and total contribution.

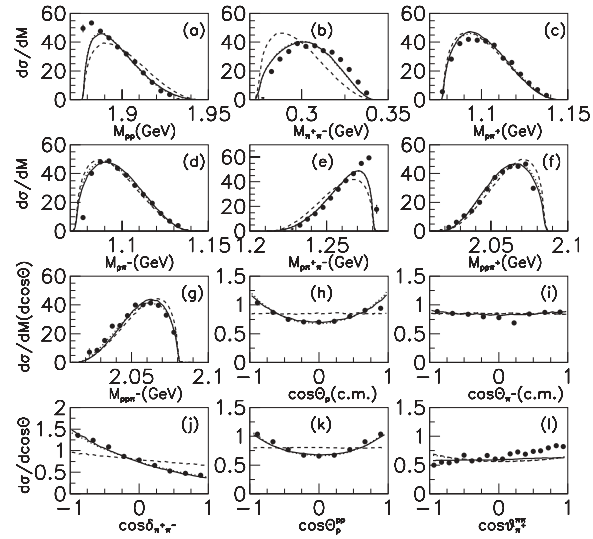

FIG. 5. Differential cross sections of $pp \to pp\pi^+\pi^-$ at beam energies 750 MeV. The dashed, dotted, and solid curves correspond to the phase space, $N^*(1440) \to N\sigma$, and full model distributions, respectively. The data are from Ref. [6].

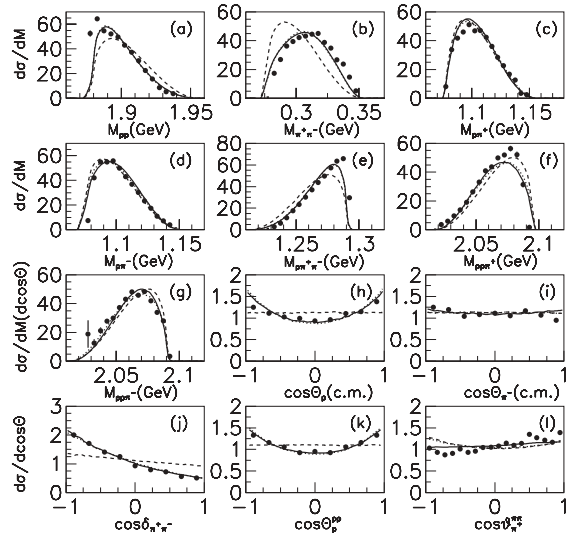

FIG. 6. Differential cross sections of $pp \to pp\pi^+\pi^-$ at beam energies 775 MeV. The meaning of the curves is the same as in Fig. 5. The data are from Ref. [6].

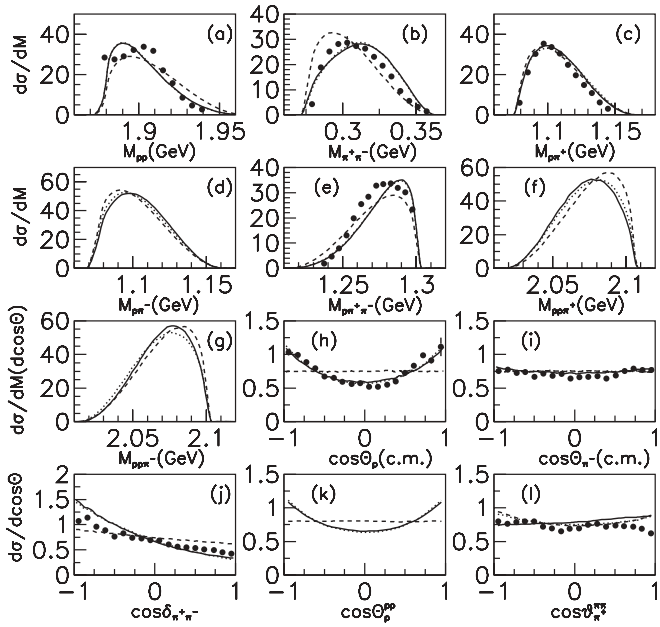

FIG. 7. Differential cross sections of $pp \to pp\pi^+\pi^-$ at beam energies 800 MeV. The meaning of the curves is the same as in Fig. 5. The data are from Ref. [9].

1360 MeV in Figs. 9 and 10 which can be tested by the measured data of CELSIUS [8]. The prominent features are the double hump structure in $M_{\pi^+\pi^-}$ and the upward bend in $\delta_{\pi^+\pi^-}$ which arise from the $N^*(1440) \to \Delta\pi$. The Valencia model gives very similar results because $M_{\pi^+\pi^-}$ and $\delta_{\pi^+\pi^-}$ are sensitive to the appearance of $N^*(1440) \to \Delta\pi$. These seem to be somewhat incompatible to the preliminary data [7,8] which show the phase space behavior in these two spectrums. The same phenomena also happen in the channel of $pp \to pp\pi^0\pi^0$ at high energies, and we will discuss them all together later.

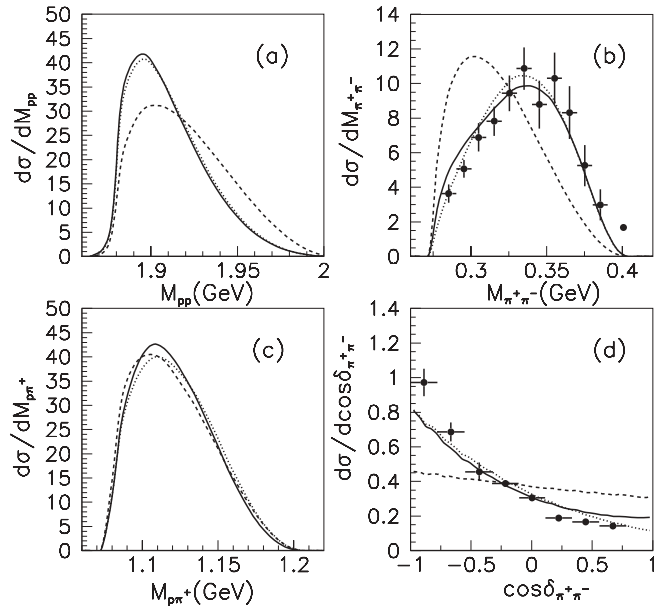

FIG. 8. Differential cross sections of $pp \to pp\pi^+\pi^-$ at beam energies 895 MeV. The meaning of the curves is the same as in Fig. 5. The preliminary data are from Ref. [8].

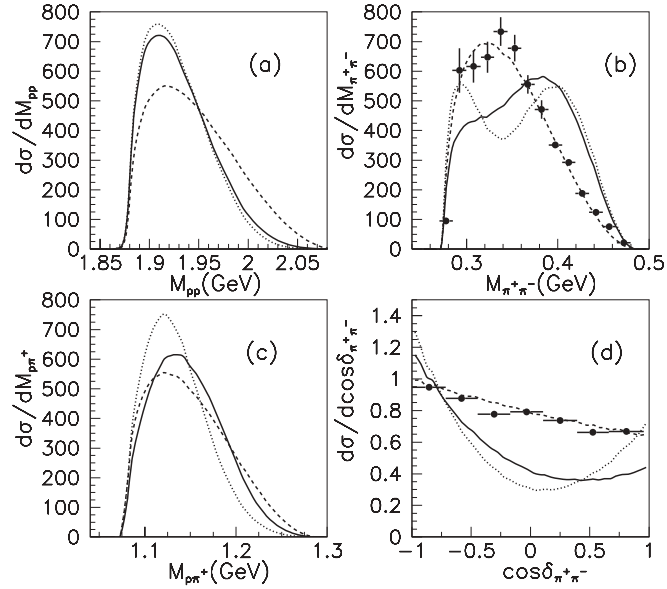

FIG. 9. Differential cross sections of $pp \to pp\pi^+\pi^-$ at beam energies 1100 MeV. The dashed, dotted, and solid curves correspond to the phase space, $N^*(1440) \to \Delta\pi$, and full model distributions, respectively. The preliminary data are from Ref. [7].

C. The channel of $pp \to pp\pi^0\pi^0$

As illustrated in Fig. 2(f), the $N^*(1440) \to N\sigma$ term dominates below 1000 MeV and the nucleon pole term also gives significant contribution below 800 MeV. The $N^*(1440) \to \Delta\pi$ and double-Δ contributions are comparable in this energy region. So it should be cautious to use this channel to extract the ratio of the partial decay widths for the decay of $N^*(1440)$. Indeed, the extracted ratios from $pp \to pp\pi^0\pi^0$ are about one-third of those from $pp \to pp\pi^+\pi^-$ at the same nominal

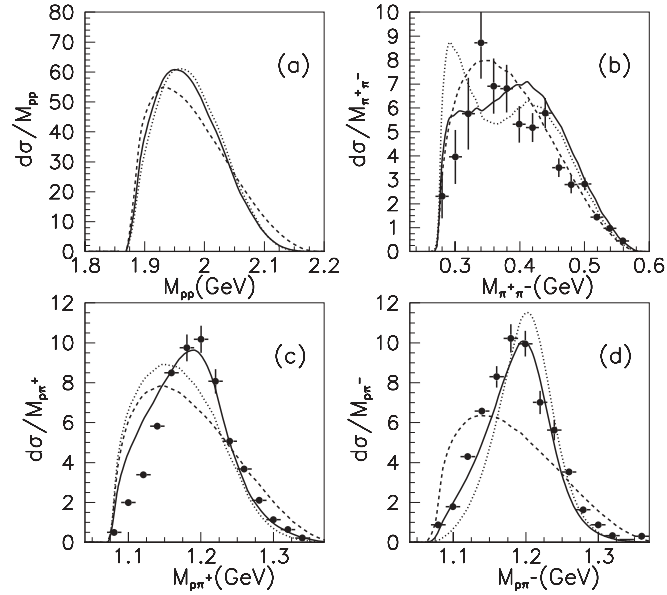

FIG. 10. Differential cross sections of $pp \to pp\pi^+\pi^-$ at beam energies 1360 MeV. The meaning of the curves is the same as in Fig. 9. The data are from Ref. [8].

mass under the assumption that $N^*(1440)$ dominates in this energy range [6,8]. The significant double-Δ and nucleon pole contributions might account for this discrepancy and their influence on the angular distributions should be reasonably considered in determining the branching ratios of $N^*(1440)$.

Above 1100 MeV, the double-Δ term dominates; the $N^*(1440) \to \Delta\pi$ and $N^*(1440) \to N\sigma$ are also important and give similar contributions. Other contributions are much smaller. The most striking feature in this energy region is that a level-off behavior happens in the total cross section between 1000 and 1200 MeV, while other channels rise smoothly when increasing the incident energy. Our model fails to describe this behavior and also overestimates the high energy data. It is possible that this shape is caused by the interference of different diagrams which are not included in our model, but this would require a peculiar energy dependence of N^* as shown by the isospin decomposition [6,8]. Another possible explanation is that there might exist a steep rise of some kind of contribution when other contributions are saturated in this energy region. This happens in the channel of $pp \to nn\pi^+\pi^+$ where a weak level-off at 1600 MeV is caused by the steep rise of $\Delta^*(1600) \to N^*(1440)\pi$. However, this is not the case for the $pp \to pp\pi^0\pi^0$ channel where $\Delta^*(1600) \to N^*(1440)\pi$ gives a much smaller contribution due to the isospin factor. So this problem is left for further clarification.

In Figs. 11–13, we show the differential cross sections of $pp \to pp\pi^0\pi^0$ at beam energies of 775, 895, and 1000 MeV, respectively. In Fig. 11, the data at 775 MeV are well reproduced and $N^*(1440) \to N\sigma$ is overwhelmingly dominant. Some of the angular distributions are sensitive to the presence of the $N^*(1440) \to \Delta\pi$ contribution, and hence can be used to determine the partial decay ratios of $N^*(1440)$, although this is somewhat complicated by the double-Δ and nucleon pole

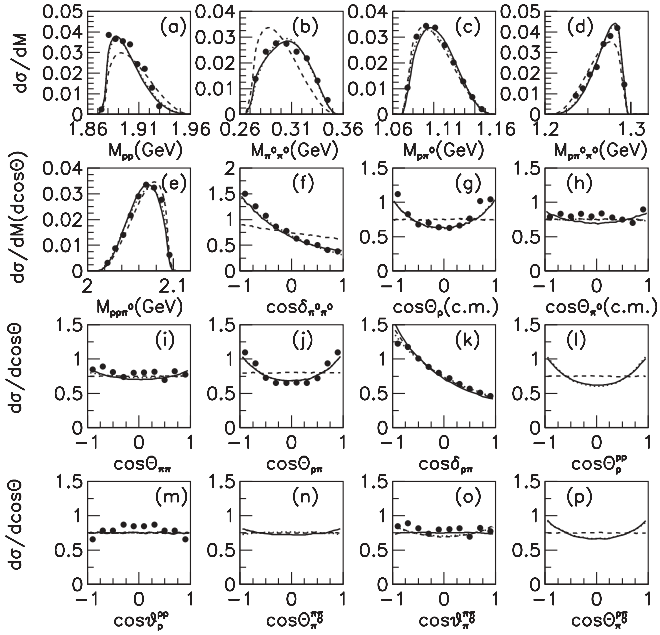

FIG. 11. Differential cross sections of $pp \to pp\pi^0\pi^0$ at beam energies 775 MeV. The meaning of the curves is the same as in Fig. 5. The data are from Ref. [8].

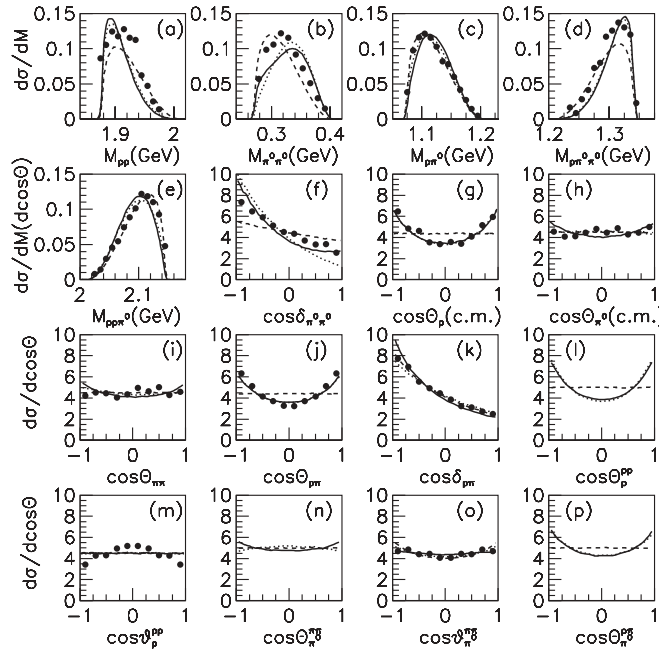

FIG. 12. Differential cross sections of $pp \to pp\pi^0\pi^0$ at beam energies 895 MeV. The meaning of the curves is the same as in Fig. 5. The data are from Ref. [8].

contributions as we pointed out earlier. The contribution of $N^*(1440) \to \Delta\pi$ and double-Δ terms become much clearer at 895 and 1000 MeV as depicted in Figs. 12 and 13, though a slight discrepancy in invariant mass spectrums at 895 MeV exists between our model and the measured data, which reminds us that it needs further improvement in the crossover

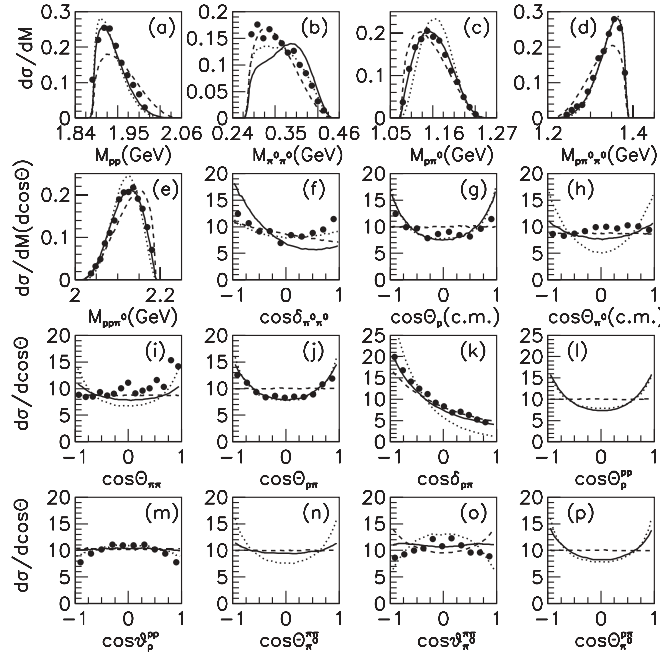

FIG. 13. Differential cross sections of $pp \to pp\pi^0\pi^0$ at beam energies 1000 MeV. The dashed, dotted, and solid curves correspond to the phase space, double-Δ, and full model distributions, respectively. The data are from Ref. [8].

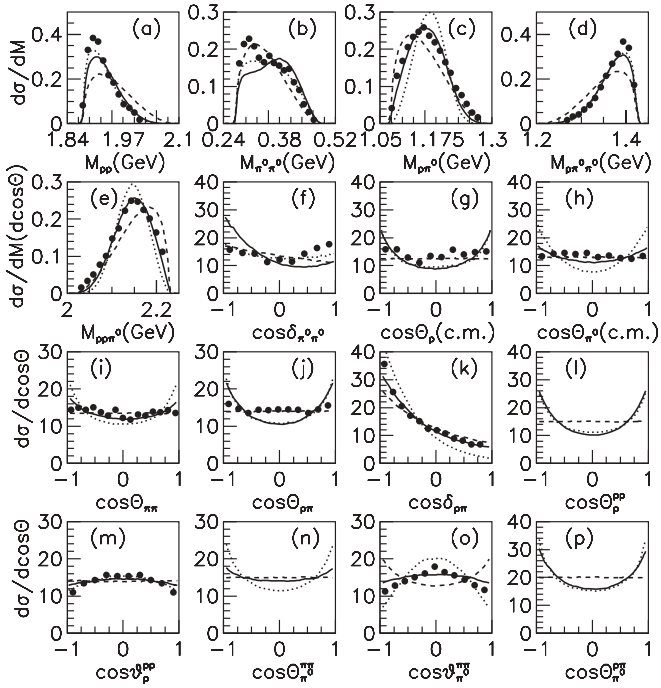

FIG. 14. Differential cross sections of $pp \to pp\pi^0\pi^0$ at beam energies 1100 MeV. The meaning of the curves is the same as in Fig. 13. The data are from Ref. [8].

region. The phase space shapes of $M_{\pi^0\pi^0}$ and $\delta_{\pi^0\pi^0}$ begin to appear at 895 MeV and up to high energies of this channel as shown in Figs. 14–16 which are the differential cross sections of $pp \to pp\pi^0\pi^0$ at 1100, 1200 and 1300 MeV. However, because the influence of the $N^*(1440) \to \Delta\pi$ does

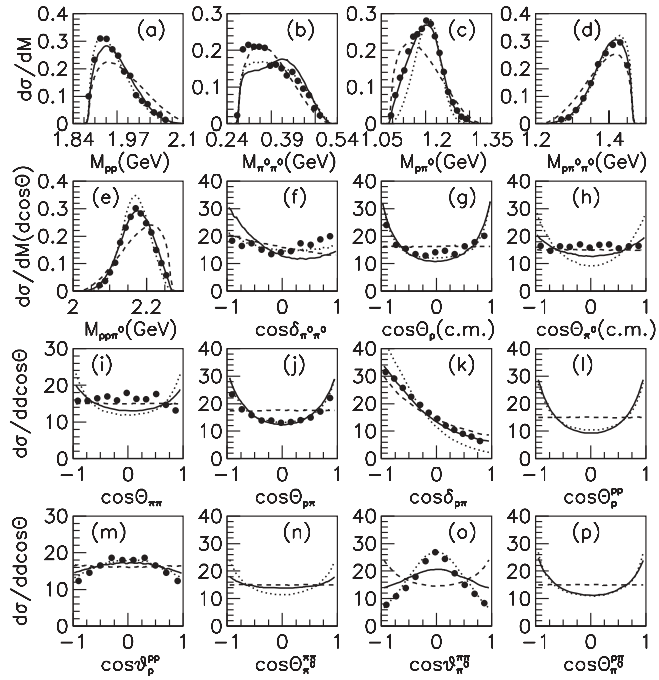

FIG. 15. Differential cross sections of $pp \to pp\pi^0\pi^0$ at beam energies 1200 MeV. The meaning of the curves is the same as in Fig. 13. The data are from Ref. [8].

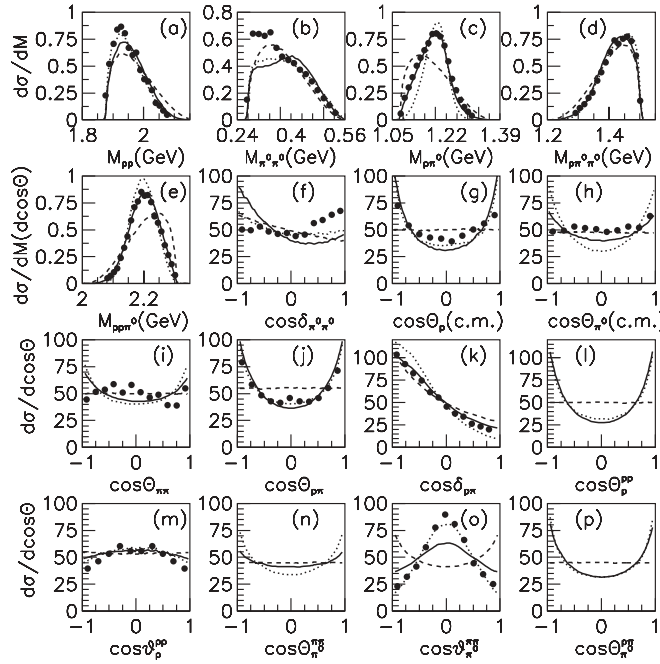

FIG. 16. Differential cross sections of $pp \to pp\pi^0\pi^0$ at beam energies 1300 MeV. The meaning of the curves is the same as in Fig. 13. The data are from Ref. [8].

not decrease much or disappear at these energies, our model gives a double hump structure in $M_{\pi^0\pi^0}$ and forward peak in $\delta_{\pi^0\pi^0}$ which are contradictory to the CELSIUS data. In order to explain the data, it is required that the $N^*(1440) \to \Delta\pi$ shows up at low energies but is immediately saturated at about 1000 MeV. That is a peculiar energy-dependence behavior which is not supported by our model. Except for $M_{\pi\pi}$ and $\delta_{\pi\pi}$, other spectrums at high energies are well fitted by our model both in $pp \to pp\pi^+\pi^-$ and $pp \to pp\pi^0\pi^0$. So we would rather conclude that something happens in the $\pi\pi$ system which needs a more thorough investigation as the next step. The π-π rescattering is found to be negligible at these energies [27].

The effect of FSI is not obvious at low energies compared to our calculated curve but enhancement seems to happen at high energies. It is possible that this is related to the behavior of the $\pi\pi$ system.

D. The channels of $pp \to pn\pi^+\pi^0$, $pn \to pp\pi^-\pi^0$, and $pn \to pn\pi^+\pi^-$

The $N^*(1440) \to N\sigma$ is not present in the $pp \to pn\pi^+\pi^0$ reaction, so the double-Δ term is the most important one in a wide energy range as shown in Fig. 2(d). The $\Delta \to \Delta\pi$ and $\Delta \to N\pi \to N\pi\pi$ terms have significant contribution below 800 MeV and also have some contribution at higher energies together with the $\Delta^*(1600)$ and $\Delta^*(1620)$ terms. The agreement with the data is very good and the FSI may influence the near-threshold region since our model slightly underestimates this part.

The channel of $pn \to pp\pi^-\pi^0$ is another reaction where the $N^*(1440) \to N\sigma$ does not contribute. Since the charged meson exchange is allowed in this channel, the $N^*(1440) \to$

$\Delta\pi$ term is very important and is of the same order as the double-Δ term in the whole energy region as can be seen in Fig. 2(e). The contributions from the nucleon pole and $\Delta \to N\pi \to NN\pi$ terms are also quite significant near the threshold. Our results reproduce the new bubble chamber data measured by KEK [10] very well, but underestimate the old data [14] by about a factor of 5. Since the double-Δ contribution has been well determined by the channel of $pp \to nn\pi^+\pi^+$, we think that the main ambiguity comes from the $N^*(1440) \to \Delta\pi$ term. If future experiments confirm the old data, then the isovector mesons like π- and ρ-meson should play more important roles in the excitation of $N^*(1440)$. On the other hand, the new data of KEK support the isoscalar excitation of $N^*(1440)$ which is favored by our model.

The $pn \to pn\pi^+\pi^-$ channel is interesting because it can shed light on the low mass enhancement in $M_{\pi\pi}$, known as the ABC effect of double-pion production in nuclear fusion reactions [28]. Below 900 MeV, the $N^*(1440) \to N\sigma$ is found to be dominant while the double-Δ and $N^*(1440) \to \Delta\pi$ terms also give some contribution as shown in Fig. 2(c). The nucleon pole and $N \to \Delta\pi$ terms are also important close to threshold. Above 1000 MeV, the double-Δ term is the most important one and the $N^*(1440)$ gives sizable contribution at high energies. The total contribution gives a reasonable description to the new KEK data while the underestimation of the data close to threshold may be due to the omission of the pn FSI. Similar to the $pn \to pp\pi^-\pi^0$ channel, our model does not favor the old bubble chamber data which need large isovector excitation of $N^*(1440)$. Very recently the ABC effect is experimentally established in $pn \to d\pi^0\pi^0$ at beam energies of 1.03 and 1.35 GeV, and has been interpreted as an s-channel double-Δ resonance [28]. According to the observation of our model, the $N^*(1440)$ emerges at these energies so it is necessary to take a further look at the mechanism of ABC effect in the $pn \to d\pi^0\pi^0$ reaction. As a matter of fact, it has been demonstrated that at beam momentum of 1.46 GeV (corresponding to beam energies of 800 MeV) where the $N^*(1440)$ is expected to be dominant, the deuteron momentum spectra can be reasonably explained by the interference of the $N^*(1440) \to N\sigma$ and $N^*(1440) \to \Delta\pi$ [12,29].

E. Final-state interaction

As discussed above, the effect of FSI is anticipated to influence the results close to threshold where the s wave is expected to be dominant. Usually the Jost function [30] is used to account for the FSI enhancement factor,

$$J(k)^{-1} = \frac{k + i\beta}{k - i\alpha}, \tag{49}$$

where k is the relative momentum of the NN subsystem in the final state. The corresponding scattering length and effective range are

$$a = \frac{\alpha + \beta}{\alpha\beta}, \quad r = \frac{2}{\alpha + \beta}, \tag{50}$$

with $a = -7.82$ fm and $r = 2.79$ fm for the $^1S_0$ pp interaction, $a = 5.42$ fm and $r = 1.76$ fm for the $^3S_1$ isoscalar pn interaction, and $a = -18.45$ fm and $r = 2.83$ fm for the $^1S_0$ nn interaction. At higher energies, the high partial waves become important and above approximate treatment would deteriorate rapidly. Fortunately, the effect of FSI should significantly decrease. So we may just ignore it above 1.4 GeV. To investigate the influence of the FSI to the energy dependence of cross sections, we assume the Jost function for the FSI and normalize this factor to the unity at the beam energy of 1.4 GeV. For the final states with the pn pair, we assume it is mainly in the $^3S_1$ isoscalar state.

Although the above prescription is quite rough, the agreement with the data is considerably improved. In Fig. 17, we demonstrate the total cross section below 1.4 GeV. The effect of FSI can be seen in some of the differential cross sections, especially NN spectrums. In Fig. 18 we take the $pp \to nn\pi^+\pi^+$ channel as a typical example. The nn FSI gives a sharp peak in the nn spectrums which agree with the $pp \to nn\pi^+\pi^+$ data. However, the data in other channels do not favor this sharp peak and this reflects the drawbacks of our formalism. The nn FSI slightly improves the fit of the $n\pi^+\pi^+$ and $nn\pi^+$ spectrums but increase the slope of $\delta_{n\pi^+}$.

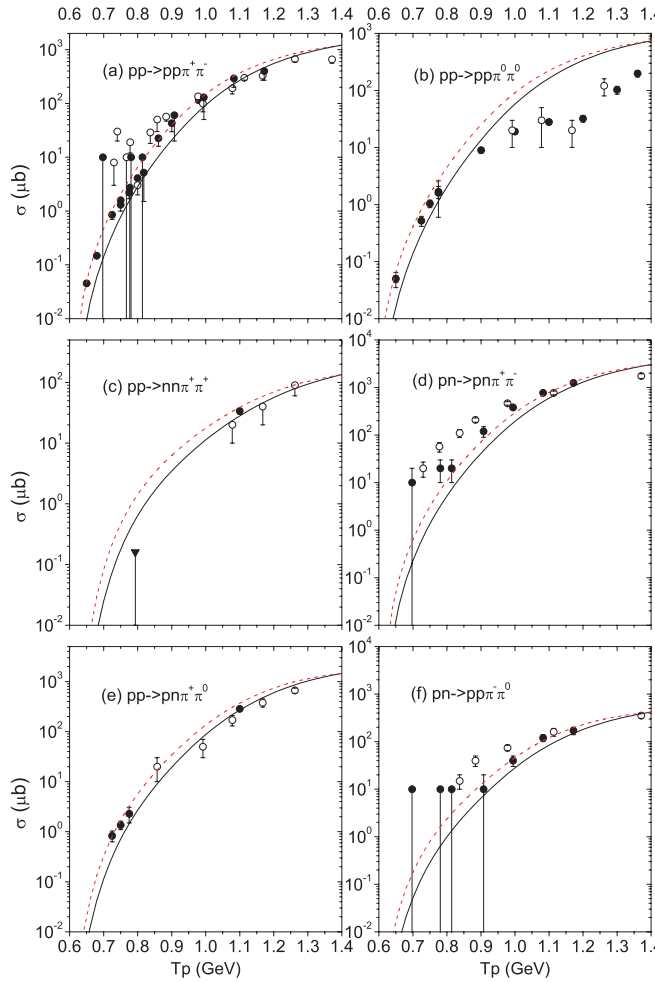

FIG. 17. (Color online) Total cross sections of $NN \to NN\pi\pi$. The black solid and red dashed curves correspond to the full contributions without and with final-state interactions, respectively. The data are the same as in Fig. 2.

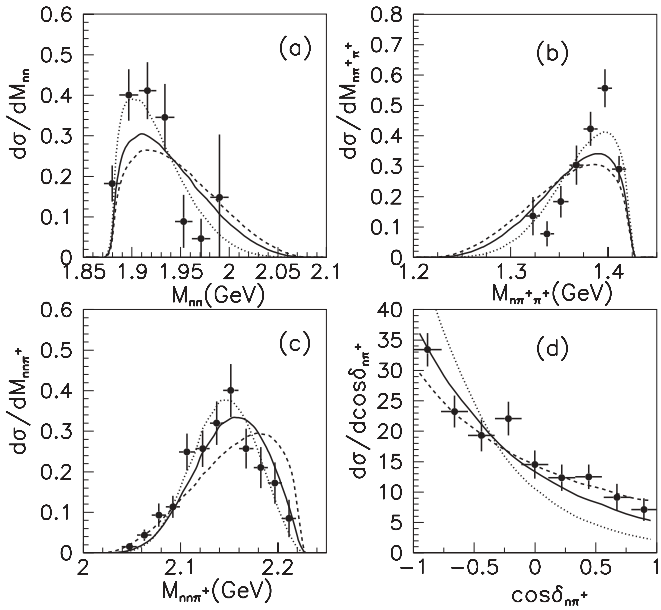

FIG. 18. Differential cross sections of $pp \to nn\pi^+\pi^+$ at beam energies 1100 MeV. The dashed, dotted, and solid curves correspond to the distributions of the phase space, the full model with and without FSI, respectively. The data are from Ref. [8].

FSI has very small influence on other angular distributions. The situations for other channels are similar.

IV. SUMMARY

In this article, we present a simultaneous analysis of various isospin channels of double-pion production in nucleon-nucleon collisions up to 2.2 GeV within an effective Lagrangian approach. We study the contributions of various resonances with mass up to 1.72 GeV and demonstrate that $N^*(1440)$, Δ, $\Delta^*(1600)$, $\Delta^*(1620)$, and nucleon pole constitute the main ingredients to reasonably explain the measured data while the contribution of other resonances are negligible. We suggest that it is necessary to consider other influences such as the double-Δ and nucleon pole contributions when one studies the properties of $N^*(1440)$ in the channels of $pp \to pp\pi^+\pi^-$ and $pp \to pp\pi^0\pi^0$. Our model gives a good description to the measured differential cross sections except some $\pi\pi$ spectra which are left as an open problem. Compared with the Valencia model, the main differences are: (1) Among three major ingredients—double-Δ, $N^*(1440) \to \Delta\pi$, and $N^*(1440) \to N\sigma$ terms—considered in the Valencia model, our model increases significantly the relative contribution from the $N^*(1440) \to N\sigma$ term by reducing the relative branching ratio of $N^*(1440) \to \Delta\pi$ and assuming a smaller cutoff parameter for the $\pi N\Delta$ coupling; (2) In addition, our model introduces significant contributions from $\Delta \to N\pi \to N\pi\pi$ at energies near threshold and from $\Delta^*(1600)$ and $\Delta^*(1620)$ at energies above 1.5 GeV. Although the model should be improved to reasonably incorporate the ISI and FSI, the conclusions reached from our model should be helpful to future experiments to be performed at COSY and HIRFL-CSR as well as further theoretical study on related problems. Our results also give hints to the ABC effect in the $pn \to d\pi^0\pi^0$ and $pd \to {}^3\mathrm{He}\pi^0\pi^0$ reactions which need to be further explored.

ACKNOWLEDGMENTS

Useful discussions with E. Oset, J. J. Xie, and Z. Ouyang are gratefully acknowledged. We also thank T. Skorodko, E. Dorochkevitch, H. Clement, and B. Höistad for providing the data files. Special thanks to C. Wilkin for careful reading of the manuscript and stimulating comments. This work was supported by the National Natural Science Foundation of China (Grant Nos. 10635080, 10875133, 10821063, 10925526, and 0701180GJ0).

[1] A. Matsuyama, T. Sato, and T.-S. H. Lee, Phys. Rep. **439**, 193 (2007); H. Kamano, B. Juliá-Díaz, T.-S. H. Lee, A. Matsuyama, and T. Sato, Phys. Rev. C **79**, 025206 (2009); M. Hirata, N. Katagiri, and T. Takaki, *ibid.* **67**, 034601 (2003); A. Fix and H. Arenhövel, Eur. Phys. J. A **25**, 115 (2005).

[2] S. Schneider, S. Krewald, and Ulf-G. Meissner, Eur. Phys. J. A **28**, 107 (2006); H. Kamano and M. Arima, Phys. Rev. C **73**, 055203 (2006); **69**, 025206 (2004).

[3] S. Strauch *et al.*, Phys. Rev. Lett. **95**, 162003 (2005); J. Ahrens *et al.*, Phys. Lett. B **624**, 173 (2005); M. Battaglieri *et al.*, Phys. Rev. D **80**, 072005 (2009); D. Krambrich *et al.*, Phys. Rev. Lett. **103**, 052002 (2009).

[4] N. Fettes, V. Bernard, and U.-G. Meissner, Nucl. Phys. A **669**, 269 (2000); V. Bernard, N. Kaiser, U.-G. Meissner, and A. Schmidt, *ibid.* **580**, 475 (1994); J. A. Gómez Tejedor and E. Oset, *ibid.* **600**, 413 (1994).

[5] M. Ripani *et al.*, Phys. Rev. Lett. **91**, 022002 (2003); G. V. Fedotov *et al.*, Phys. Rev. C **79**, 015204 (2009); V. I. Mokeev, V. D. Burkert, T. S. H. Lee, L. Elouadrhiri, G. V. Fedotov, and B. S. Ishkhanov, *ibid.* **80**, 045212 (2009).

[6] J. Johanson *et al.*, Nucl. Phys. A **712**, 75 (2002); W. Brodowski *et al.*, Phys. Rev. Lett. **88**, 192301 (2002); J. Pätzold *et al.*, Phys. Rev. C **67**, 052202(R) (2003); E. Doroshkevich *et al.*, Eur. Phys. J. A **18**, 171 (2003); T. Skorodko *et al.*, *ibid.* **35**, 317 (2008); Phys. Lett. B **679**, 30 (2009).

[7] H. Clement *et al.*, Int. J. Mod. Phys. A **20**, 1747 (2005).

[8] T. Skorodko, Ph.D. thesis, University of Tübingen, Tübingen, Germany, 2009.

[9] S. Abd El-Bary *et al.*, Eur. Phys. J. A **37**, 267 (2008); S. Abd El-Samad *et al.*, *ibid.* **42**, 159 (2009).

[10] T. Tsuboyama, F. Sai, N. Katayama, T. Kishida, and S. S. Yamamoto, Phys. Rev. C **62**, 034001 (2000).

[11] V. V. Sarantsev *et al.*, Phys. At. Nucl. **70**, 1885 (2007).

[12] L. Alvarez-Ruso, E. Oset, and E. Hernández, Nucl. Phys. A **633**, 519 (1998); L. Alvarez-Ruso, Ph.D. thesis, University of Valencia, Valencia, Spain, 1999.

[13] E. Ferrari, Nuovo Cimento **30**, 240 (1963); E. Ferrari, S. Gennarini, and P. Lariccia, *ibid.* **39**, 169 (1965).

[14] E. Pickup, D. K. Robinson, and E. O. Salant, Phys. Rev. **125**, 2091 (1962); E. L. Hart *et al.*, *ibid.* **126**, 747 (1962); A. M. Eisner *et al.*, *ibid.* **138**, B670 (1965);

D. C. Brunt *et al.*, *ibid.* **187**, 1856 (1969); D. R. F. Cochran *et al.*, Phys. Rev. D **6**, 3085 (1972); F. Shimizu *et al.*, Nucl. Phys. A **386**, 571 (1982); F. H. Cverna, P. R. Bevington, M. W. McNaughton, H. B. Willard, N. S. P. King, and D. R. Giebink, Phys. Rev. C **23**, 1698 (1981); L. G. Dakhno *et al.*, Sov. J. Nucl. Phys. **37**, 540 (1983).

[15] C. Amsler *et al.*, Phys. Lett. B **667**, 1 (2008).

[16] R. Machleidt, K. Holinde, and C. Elster, Phys. Rep. **149**, 1 (1987); R. Machleidt, Adv. Nucl. Phys. **19**, 189 (1989).

[17] K. Tsushima, A. Sibirtsev, A. W. Thomas, and G. Q. Li, Phys. Rev. C **59**, 369 (1999); **61**, 029903(E) (2000).

[18] A. Engel, R. Shyam, U. Mosel, and A. K. Dutt-Mazumder, Nucl. Phys. A **603**, 387 (1996).

[19] B.-S. Zou and F. Hussain, Phys. Rev. C **67**, 015204 (2003).

[20] Z. Ouyang, J.-J. Xie, B.-S. Zou, and H.-S. Xu, Nucl. Phys. A **821**, 220 (2009); Int. J. Mod. Phys. E **18**, 281 (2009).

[21] B.-S. Zou, and D. V. Bugg, Eur. Phys. J. A **16**, 537 (2003).

[22] C. Schütz, J. Haidenbauer, J. Speth, and J. W. Durso, Phys. Rev. C **57**, 1464 (1998).

[23] J.-J. Xie, C. Wilkin, and B.-S. Zou, Phys. Rev. C **77**, 058202 (2008).

[24] A. V. Sarantsev *et al.*, Phys. Lett. B **659**, 94 (2008).

[25] [http://cernlib.web.cern.ch/cernlib/libraries.html].

[26] H. P. Morsch *et al.*, Phys. Rev. Lett. **69**, 1336 (1992); E. Hernández and E. Oset, Phys. Rev. C **60**, 025204 (1999); O. Krehl, C. Hanhart, S. Krewald, and J. Speth, *ibid.* **62**, 025207 (2000); E. Hernández, E. Oset, and M. J. Vicente Vacas, *ibid.* **66**, 065201 (2002).

[27] P. Lebiedowicz, A. Szczurek, and R. Kaminski, Phys. Lett. B **680**, 459 (2009).

[28] M. Bashkanov *et al.*, Phys. Lett. B **637**, 223 (2006); Phys. Rev. Lett. **102**, 052301 (2009); S. Dymov *et al.*, *ibid.* **102**, 192301 (2009).

[29] L. Alvarez-Ruso, Phys. Lett. B **452**, 207 (1999).

[30] M. Goldberger and K. M. Watson, *Collision Theory* (Wiley, New York, 1964).